Establishment and application of the 0/45 reflectance factor scale over the shortwave infrared

Catherine C. Cooksey, David W. Allen, Benjamin K. Tsai, and Howard W. Yoon

National Institute of Standards and Technology,100 Bureau Drive, Gaithersburg, MD 20899
**Corresponding author: catherine.cooksey@nist.gov*

Received Month X, XXXX; revised Month X, XXXX; accepted Month X, XXXX; posted Month X, XXXX (Doc. ID XXXXX); published Month X, XXXX

This paper describes the establishment and application of the 0/45 reflectance factor scale in the shortwave infrared (SWIR) from 1100 nm to 2500 nm. Design, characterization, and the demonstration of a 4-stage, extended indium-gallium-arsenide radiometer to perform reflectance measurements in the SWIR have been previously discussed. Here, we focus on the incorporation of the radiometer into the national reference reflectometer, its validation through comparison measurements, and the uncertainty budget. Next, this capability is applied to the measurement of three different diffuser materials. The 0/45 spectral reflectance factors for these materials are reported and compared to their respective 6/di spectral reflectance factors.

OCIS codes: (120.1840) Densitometers, reflectometers; (120.5700) Reflection; (290.1483) BSDF, BRDF, and BTDF; (280.0280) Remote sensing and sensors;
http://dx.doi/org/10.1364/AO.99.099999

1. Introduction

Optical spectrometers often rely on the use of white diffuse reflectance standards, such as sintered polytetrafluoroethylene (PTFE), as references in measuring reflectance or transferring a scale of radiance. An important application of such spectrometers is Earth remote sensing. As the field of Earth remote sensing has evolved and produced more advanced sensors, the data products have also advanced to become indispensable tools for monitoring the environment, particularly the small decadal-scale changes associated with climate change. With these advances has come the need for reducing the overall measurement uncertainty. For many applications, traceability to a national metrology laboratory is motivated by the need to relate the measurements to an absolute scale accepted internationally.

For over two decades, the National Institute of Standards and Technology (NIST) has disseminated the scale of reflectance through calibrated standards provided by the Spectral Tri-function Automated Reference Reflectometer (STARR). This reference instrument provides reflectance measurements for both directional-hemispherical and bidirectional measurement geometries. These geometries define the direction or range of directions by which a material is illuminated and the reflected light is collected. The geometry of a reflectance measurement is designated by its incident angle θ_i and detection angle θ_r as θ_i/θ_r [1]. For example, a bidirectional geometry in which the sample is illuminated at 0° from its normal and the reflected radiant flux is detected at an angle 45° from the normal is referred to as 0/45. For the case of a directional-hemispherical geometry, the sample is illuminated at a given incident angle θ_i and the reflected light is collected over the full hemisphere above the sample using an integrating sphere. Thus, a directional-hemispherical geometry in which the sample is illuminated at 6° from its normal is designated 6/di (where "d" indicates diffuse and "i" indicates that the specular component is *included* in the measurement).

While the directional-hemispherical measurements have been routinely provided in the 250 nm to 2500 nm spectral range (often referred to as the solar reflective region), the bidirectional measurements have primarily been limited to the 250 nm to 1100 nm spectral range of the silicon photodiode. In general, this is due to the lack of a detector that can operate over the 1000 nm to 2500 nm spectral range with a signal-to-noise ratio, dynamic range, and linearity comparable to that of the silicon photodiode. The use of a radiometer, which integrates a thermally-cooled extended indium-gallium-arsenide (ex-InGaAs) photodiode with a low-noise preamplifier developed at NIST, has provided a means for extending the spectral range with acceptable performance.

The design, characterization, and potential of a 4-stage ex-InGaAs radiometer to make reflectance measurements in the shortwave infrared (SWIR) have been previously discussed in Reference 2. In this paper, we focus on the incorporation of this radiometer into the STARR, its validation through comparison measurements, and the uncertainty budget. We also apply this capability to the measurement of three different diffuser materials. The 0/45 spectral reflectance factors for these materials are reported and compared to their respective 6/di spectral reflectance factors.

2. Shortwave Infrared Measurements with an Extended InGaAs Radiometer

A. Measurement of Bidirectional Reflectance Factors

STARR is used to maintain and disseminate the national reference scale for bidirectional reflectance. It acquires absolute measurements of bidirectional reflectance using a monochromatic source (nominal bandwidth of 14 nm) for illumination of the sample and broadband detection of the reflected radiation. STARR is described extensively in Reference 3, and a diagram is shown in Figure 1.

Briefly, the incident radiant flux is produced by a lamp-based source (a xenon arc lamp for wavelengths of 400 nm and shorter and a quartz-tungsten-halogen incandescent lamp for longer wavelengths). Radiant flux produced by the source is focused through an order-sorting filter and shutter onto the entrance slit of a single-grating monochromator. The beam emerging from the exit slit of the monochromator is spatially filtered by an iris to provide a circular incident beam on the sample and is collimated by an off-axis parabolic mirror, resulting in a nominal diameter of 17 mm for the sampling aperture. Next, the resulting beam passes through a Glan-Taylor polarizer before passing through the sample goniometer. The beam is collected by the receiver aperture of the radiometer, and is focused by a lens onto the radiometer, which produces a signal proportional to the radiant flux.

The bidirectional reflectance is calculated from the measured signals in terms of reflectance factor, which is defined as the ratio of radiant flux reflected by a sample to that reflected by a perfectly reflecting diffuser under identical geometrical measurement conditions. A perfectly reflecting diffuser (a theoretical concept) describes a material that reflects incoming radiation without loss and with a Lambertian distribution. Thus, the more closely a material mimics a perfectly reflecting diffuser, the more closely its reflectance factor will be to one.

The spectral reflectance factor for a given sample (depicted as a reflectance panel in Figure 1) is calculated using on the following equation:

$$R(\lambda,\sigma) = \frac{\pi \cdot d^2}{A \cdot \cos\theta_r} \cdot \frac{S_r\ (\lambda,\sigma)}{S_i\ (\lambda,\sigma)} \cdot \eta \qquad (1)$$

where $R(\lambda,\sigma)$ is the reflectance factor for a given wavelength λ and polarization σ, d is the distance between the sample and the aperture of the receiver, A is the area of this aperture, and θ_r is the detection angle of the reflected radiant flux. $S_r(\lambda)$ is the net signal due to the reflected radiant flux and $S_i(\lambda)$ is the net signal due to the incident radiant flux, such that both signals are corrected for the dark current. η is the gain factor correction between the two signals.

The reflected and incident signals are collected by rotating the radiometer between the reflected position and the incident position. When the radiometer is in the reflected position, the sample is centered in the incident beam path; when the radiometer is in the incident position, the sample is shifted out of the incident beam path. For each wavelength and polarization, the signals are collected in the following sequence: incident signal, dark signal in the incident position, reflected signal, dark signal in the reflected position, incident signal, and dark signal in the incident position. For detection with the silicon radiometer and picoammeter, dark signals are obtained by closing the shutter on the monochromator, and the net signals for the incident and reflected positions are obtained by subtracting the dark signals. For detection with the ex-InGaAs radiometer, the signals are collected in AC mode using a mechanical chopper and phase-sensitive detection. The average net signal due to the incident radiant flux, acquired before and after each measurement of the reflected signal, is used to minimize the effects of source drift and fluctuations on the timescale of a single reflectance measurement. The values for both polarizations are averaged to yield the reflectance factor for unpolarized incident radiant flux.

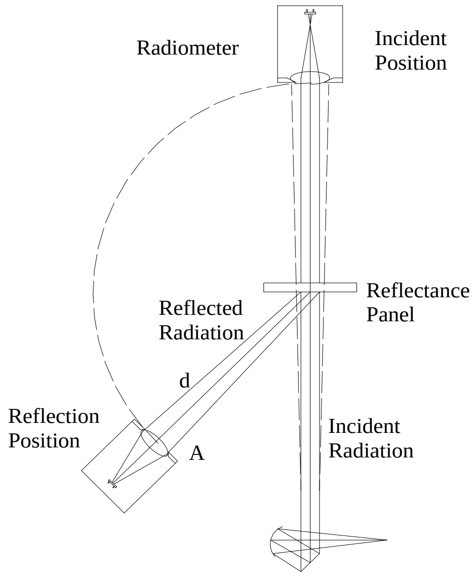

Fig. 1. Measurement scheme of STARR. The illuminator, consisting of the lamp-based source and monochromator, is not shown for simplification.

B. SWIR Radiometer Design

STARR was originally designed to acquire bidirectional reflectance measurements using a radiometer with an ultraviolet-enhanced silicon photodiode. Based on the output power of the monochromator and the spectral responsivity of this radiometer, measurement of bidirectional reflectance was limited to the spectral range from 250 nm to 1100 nm. However, the development of the ex-InGaAs radiometer with low noise and high-shunt resistance has made possible the extension of the bidirectional reflectance scale into the shortwave infrared [4].

A radiometer incorporating an ex-InGaAs photodiode was described in Reference 2. Briefly, the radiometer consists of a 4-stage thermo-electrically cooled ex-InGaAs photodiode, a low noise preamplifier, an aperture, and a refractive lens. The lens is a 25 mm diameter, bi-convex calcium fluoride singlet lens with a 50 mm focal length, which collects the radiant flux and focuses it onto the 3 mm diameter active area of the ex-InGaAs photodiode. The photodiode is cooled to approximately –55 °C. The temperature of the radiometer body is stabilized using an external chiller connected to the heat-sink of the thermoelectric cooler with a set point of 19 °C. An aperture is placed directly in front of the lens. The radius of the aperture, which is used to evaluate the area A in Equation 1, was measured by the NIST Aperture Area Facility and was determined to be 10.17763 mm with a relative standard uncertainty $u(r)$ of 0.007 %. The distance, d in Equation 1, between the sample and the aperture of the receiver is 560.4 mm with an uncertainty $u(D)$ of 0.3 mm.

C. Validation of 0/45 reflectance factor scale

Bidirectional reflectance measurements made using the ex-InGaAs radiometer were validated through a comparison measurement with the NIST Irradiance Scale Realization Facility (ISRF) [2]. At this facility, the 0/45 reflectance factor of a given sample can be determined through a comparison measurement using a source of known spectral irradiance and a source of calibrated spectral radiance. A diagram of the ISRF is shown in Figure 2.

Briefly, the spectroradiometer is moved to image the tungsten-strip lamp which is placed in the radiance position. The spectral radiances of the tungsten-strip lamp are separately assigned using a blackbody with known temperatures [5]. After the radiance responsivity of the spectroradiometer has been calibrated, the spectroradiometer is moved over to measure the spectral radiances from the plaque (depicted by the reflectance panel in Figure 2). An FEL lamp of known spectral irradiance illuminates the plaque in the 0° incident direction [6]. The FEL lamp is set at a distance of 50 cm from the front surface of the plaque to minimize the additional uncertainties from distance corrections to the incident spectral irradiances. A rectangular area, 2 cm wide by 3 cm high, on the plaque is imaged by the spectroradiometer. The differences of the spectral irradiances over the larger 2 cm by 3 cm rectangular area to the 1 cm circular area, where the FEL lamps are calibrated, are estimated to be 0.25 % from angular scans of other FEL lamps. The reflected radiation is collected at a detection angle of 45° by the spectroradiometer. The 0/45 reflectance factor of the sample is then calculated using

$$R(\lambda) = \pi \cdot \frac{L_r}{E_i} \cdot \eta \qquad (2)$$

where L_r is the radiance from the reflectance panel, E_i is the incident irradiance, and η is the gain factor correction for the two radiances.

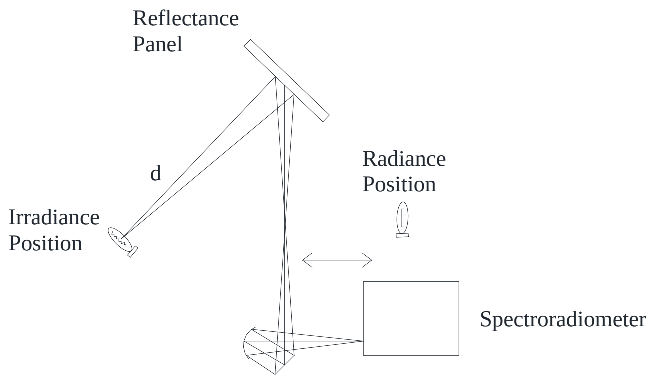

Fig. 2. Measurement scheme of the ISRF.

The 0/45 reflectance factors from 1000 nm to 2500 nm of a sintered PTFE standard were determined independently using STARR and ISRF. The results are shown in Figure 3 along with the 0/45 reflectance factors obtained using STARR with the silicon radiometer in the region from 1000 nm to 1100 nm where its useful coverage overlaps with that of the ex-InGaAs radiometer. Although the measurement wavelengths in the ISRF are limited due to the limited number of calibration wavelengths of the radiance and the irradiance standards, agreement is achieved both on a point-by-point basis and spectrally across the SWIR. Quantitatively, agreement between two measurements is assessed by comparing the difference between the measurements to the combined expanded uncertainty ($k = 2$) of the difference. The differences between the measurements obtained by STARR with the ex-InGaAs radiometer and ISRF are well within the uncertainty of differences, which is 0.012. Similarly, the differences between the measurements obtained by STARR with the ex-InGaAs radiometer and the silicon radiometer are within the uncertainty of differences, which is 0.008. Together, these two data sets validate the 0/45 reflectance factor scale realized on STARR with the ex-InGaAs radiometer.

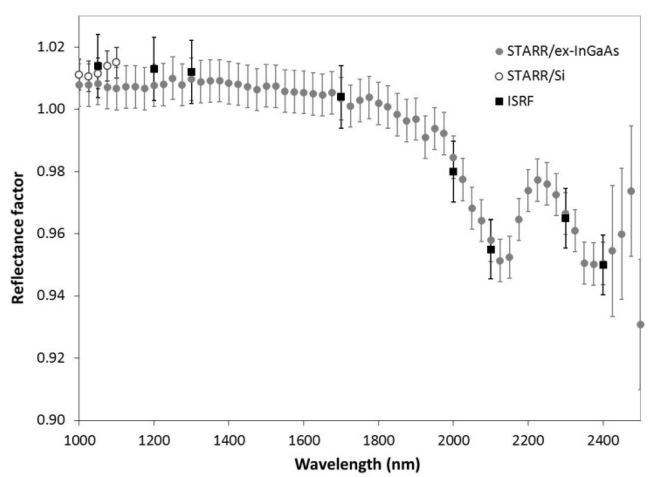

Fig. 3. Plot of 0/45 reflectance factors with expanded uncertainties ($k = 2$) for a sintered PTFE standard obtained using STARR and IRSF.

D. Uncertainty Budget

STARR has a well-established and validated uncertainty budget for bidirectional reflectance measurements [3]. The contributions of each source of uncertainty are calculated in accordance with the procedures outlined in References 7 and 8. Here, we have extended that budget to include the specifics for the longer wavelength measurements using ex-InGaAs radiometer. This budget considers additional uncertainty components, not previously assessed in Reference 2.

The sources of uncertainty, which are not dependent on the sample, are aperture distance, aperture area, viewing angle, solid angle calculation, sample location (offset of the sample plane with respect to the axis of sample rotation), radiometer linearity, radiometer gain ratio, and repeatability. The first three sources appear explicitly in the measurement equation (Equation 1). Their sensitivity coefficients are determined from the first derivative of the measurement equation with respect to the given variable. Their contributions to the uncertainty are evaluated, for their nominal values, from the product of their respective sensitivity coefficients and standard uncertainties. The uncertainties for the later components were evaluated as part of the characterization of the STARR instrument.

The sample-dependent sources of uncertainty are wavelength, sample uniformity, and sample alignment. The uncertainty caused by wavelength is evaluated from the derivative of the reflectance factor with respect to wavelength. The uncertainty caused by sample uniformity was evaluated from reflectance signals measured at 5 mm displacements, both horizontal and vertical, from the nominal center of the sample, while the uncertainty in the sample alignment is evaluated from reflectance factors measured at angles in increments of 0.1° around the nominal incident angle.

All the uncertainty components are assumed to have normal probability distributions. The combined uncertainty is the square root of the sum of squares of the contributions of the uncertainty components. The final uncertainty is the expanded measurement uncertainty, which is obtained by multiplying the combined uncertainty by the coverage factor $k = 2$.

Table 1 lists the sources of uncertainty and uncertainty contributions for 0/45 reflectance factor measurements from 1000 nm to 2500 nm. The contributions provided for sample dependent components are typical for sintered PTFE standards, such as the one depicted in Figure 3.

One of the most significant contributors to the expanded uncertainty is radiometer linearity. This component encompasses the whole detection system, including the photodiode and preamplifier. It was determined using the beam-addition method with a double-aperture assembly [9]. The increased value of this uncertainty component for the ex-InGaAs radiometer compared to the silicon radiometer (0.1 %) may be related to the non-uniformity of the photodiode. Overall, the resulting expanded uncertainty in the SWIR compares well with the nominal expanded uncertainty of 0.5 % for sintered PTFE standards obtained using STARR with the silicon radiometer. The larger uncertainty occurring beyond 2400 nm is due to a combination of decreasing radiant flux produced by the lamp sources and decreasing radiometer responsivity.

Table 1. Uncertainty budget for 0/45 reflectance factor values obtained using STARR with an ex-InGaAs radiometer.

Source of Uncertainty	Standard Uncertainty	Uncertainty Contribution
Aperture Distance	0.3 mm	0.11%
Aperture Area	0.046 mm²	0.014 %
Viewing Angle	0.06°	0.1%
Solid Angle Calculation		0.05%
Sample Location	0.3 mm	0.07 %
Radiometer Gain Ratio		0.06 %
Radiometer Linearity		0.2 %
Repeatability		0.12 % (1100 nm < $\lambda \leq$ 2400 nm)
		1.0 % (2400 nm < $\lambda \leq$ 2500 nm)
Wavelength*	1 nm	< 0.01% (1100 nm < $\lambda \leq$ 2000 nm)
		0.03% (2000 nm < $\lambda \leq$ 2500 nm)
Sample Uniformity*	0.001	0.15%
Sample Alignment*	0.1°	0.02%
		Expanded Uncertainty ($k = 2$)
		0.7 % (1100 nm < $\lambda \leq$ 2000 nm)
		0.7 % (2000 nm < $\lambda \leq$ 2400 nm)
		2.1 % (2400 nm < $\lambda \leq$ 2500 nm)

*Contributions for sample dependent components are typical for sintered PTFE standards.

3. 0/45 Reflectance Factors for Several Diffuse Reflectance Standards

This new capability of measuring 0/45 reflectance factors in the SWIR was applied to three different diffuser materials: sintered PTFE, pressed PTFE, and ceramic. Both forms of PTFE are commonly used as material for reflectance standards. The ceramic material used in this comparison was chosen because it was designed to reflect light across the solar reflective region at a similar level as sintered PTFE. The composition of the ceramic (AHP99) is 99 % alumina (Al_2O_3) and 1% of a proprietary silicate glass, which is used to bind the Al_2O_3 particles during kiln firing. The ceramic is known to have minimal fluorescence, centered at approximately 690 nm, likely due to chromium ion impurities [10]. Based on exploratory studies at NIST, the contribution of fluorescence to the total light reflected is greatest with UV excitation and decreases to a negligible amount by 650 nm. (The fluorescence contribution appears to be somewhat sample dependent and is approximately 1 % at 300 nm and 0.1 % to 0.3 % at 500 nm.) This ceramic has a matte finish and is not known to attract particulate contamination as a result of electrostatic charge.

Figure 4 shows the results of the 0/45 reflectance factor measurements for the diffuser materials over the range from 250 nm to 2500 nm. The expanded uncertainties ($k = 2$) for these measurements are given in Table 2. Throughout much of the spectral region shown in Figure 4, all three materials perform similarly in terms of their 0/45 reflectance factors. For wavelengths less than 600 nm, the 0/45 reflectance factors for the ceramic sample are significantly reduced compared to the PTFE samples. However, for wavelengths greater than 2000 nm, the reflectance factors for the ceramic sample are less wavelength dependent than the PTFE samples. Overall, the expanded uncertainties differ little for the three materials.

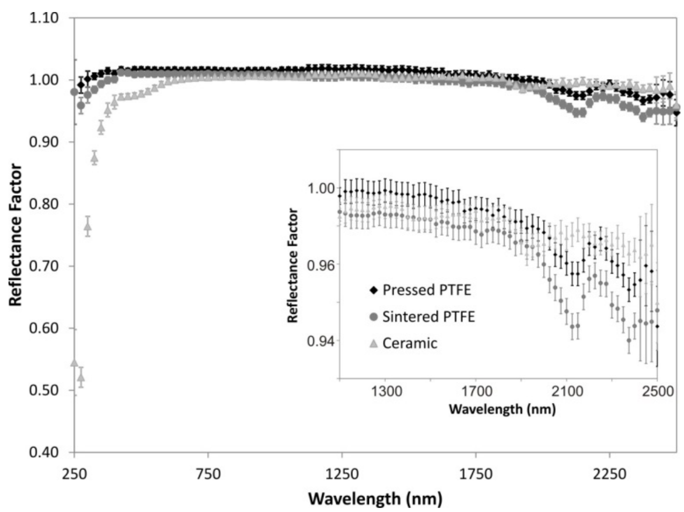

Fig. 4. 0/45 spectral reflectance factor R as a function of wavelength λ of sintered PTFE, pressed PTFE, and ceramic samples. The inset depicts the shortwave infrared region in finer detail.

Table 2. Expanded uncertainty ($k = 2$) of the 0/45 spectral reflectance of sintered PTFE, pressed PTFE, and ceramic samples.

Expanded Uncertainty ($k = 2$)	Sintered PTFE	Pressed PTFE	Ceramic
λ = 250 nm	0.052	0.052	0.053
275 nm ≤ λ ≤ 300 nm	0.013	0.013	0.016
325 nm ≤ λ ≤ 400 nm	0.0056	0.0052	0.011
425 nm ≤ λ ≤ 1100 nm	0.0049	0.0044	0.0043
1125 nm ≤ λ ≤ 2000 nm	0.0065	0.0062	0.0061
2025 nm ≤ λ ≤ 2400 nm	0.0065	0.0062	0.0062
2425 nm ≤ λ ≤ 2500 nm	0.021	0.021	0.021

4. Comparison of the 0/45 and 6/di reflectance factor scales

Because the 0/45 reflectance factor scale has been limited due to the availability of detectors (wavelengths less than 1100 nm for silicon radiometers, such as used in the NIST STARR facility, or less than 1700 nm for indium-gallium-arsenide radiometers found in other facilities [11,12]), the reflectance properties of materials in the SWIR are frequently determined using a directional-hemispherical geometry. This geometry uses an integrating sphere to collect all of the radiative flux reflected from the material. For nearly Lambertian materials, it is common practice to approximate the difference between the 0/45 reflectance factor and the directional-hemispherical reflectance factor by a small, wavelength-independent offset. Thus, the spectrum obtain in the SWIR with a directional-hemispherical geometry is shifted to vertically align with the 0/45 measurements. Now, using the ex-InGaAs radiometer, we can measure the 0/45 reflectance factors directly and compare the results with those obtained using the directional-hemispherical geometry.

A. Measurement of Directional-Hemispherical Reflectance Factors

Directional-hemispherical measurements were acquired using STARR [3]. Briefly, the unpolarized radiant flux, which is produced by the lamp-based source and monochromator described in Section 2, passes through the entrance port of an integrating sphere. The sphere has a diameter of 30 cm, is lined with a 1 cm thick coating of polytetrafluoroethylene (PTFE), and has a sample port with a diameter of 5 cm. Inside the sphere, the beam is incident upon either the sample (sample position) or the wall of the sphere (wall position) at an angle of illumination of 6° from the normal of the surface. The sampling aperture has a diameter of 25 mm, as defined by the illumination beam. The reflected radiant flux of the beam undergoes multiple reflections (> 100) within the integrating sphere, achieving uniform irradiance on the sphere wall. A detector attached to the integrating sphere views a large portion of the sphere wall, producing a signal proportional to the reflected flux of either the sample or the wall, depending on the incident beam position. The detector is an ultraviolet-enhanced silicon photodiode for wavelengths less than 1100 nm and a 2-stage thermo-electrically cooled, ex-InGaAs photodiode for longer wavelengths.

Measurements acquired using an illumination angle of 6° include the specular component of the reflected radiant flux. This geometry is designated as 6/di. The 6/di spectral reflectance factors of a sample are determined by a relative measurement using the following equation:

$$R(\lambda) = \frac{S(\lambda)}{S_{\mathrm{w}}(\lambda)} \cdot \frac{S_{\mathrm{w,s}}(\lambda)}{S_{\mathrm{s}}(\lambda)} \cdot R_{\mathrm{s}}(\lambda) \qquad (3)$$

where S is the net signal from the reflected radiant flux from the sample, S_w is the net signal from the reflected radiant flux from the wall when the sample is at the sample port, $S_{w,s}$ is the net signal from the reflected radiant flux from the wall when the standard is at the sample port, S_s is the net signal from the reflected radiant flux from the reference standard, and R_s is the directional-hemispherical spectral reflectance factor of the reference standard. The reference standard is pressed PTFE, and its 6/di spectral reflectance factors have been determined previously using the absolute method of Van den Akker [13,14].

This measurement is accomplished using the substitution method. First, the reference standard is installed at the sample port of the integrating sphere. For each wavelength, the following signals were measured in this order: wall signal, dark signal in the wall position, reference standard signal (in the sample position), dark signal in the sample position, wall signal, and dark signal in the wall position. Next, the sample is installed at the sample port. The following signals were measured for each wavelength in this order: sample signal, dark signal in the sample position, wall signal, and dark signal in the wall position, sample signal, and dark signal in the sample position. For detection with a silicon photodiode and picoammeter, dark signals were obtained by closing the shutter on the monochromator. For detection with an ex-InGaAs photodiode, the signals are collected in AC mode using a mechanical chopper and phase-sensitive detection.

B. Comparison results

The 6/di reflectance factors of the three diffuser materials described in Section 3 were measured from 250 nm to 2500 nm in 25 nm increments and compared to their respective 0/45 reflectance factors. Figure 5 shows how the ratio of 0/45 reflectance factor to 6/di reflectance factor differs from one. While there appears to be a constant offset for all three materials between the two geometries from 400 nm to 1100 nm, the ratios clearly decrease for wavelengths longer than 1100 nm, with sintered PTFE experiencing the greatest decline.

The ratios of 0/45 reflectance factor to 6/di reflectance factors for each material were fit to a line using a linear least-squares method. Only the ratios within the spectral range of 400 nm to 2500 nm were used for the fit, and the inverse of the uncertainties squared were used as weights for the fitting process. The resulting coefficients for the least-squares fits and their uncertainties ($k = 2$) are provided in Table 3.

Thus, for those who wish to approximate the 0/45 reflectance factors of nearly Lambertian materials in the SWIR with reflectance factors obtained using a directional-hemispherical geometry, a wavelength-dependent correction factor will need to be applied. The correction factor is determined from the linear fits, and the overall uncertainty of that correction factor is determined from prediction bands.

A prediction band is the estimated interval within which a future observation will fall, for a given probability, based on the data that has already been observed [16]. (The expanded uncertainty of the least-squares fit describes the mean fit dispersion, not the sample population.) Prediction bands were calculated for a confidence level of 95 % based on the sample of ratios and their linear fits. The fits and prediction bands are shown in Figure 6. The resulting prediction bands are approximately 0.011 for pressed PTFE, 0.006 for sintered PTFE, and 0.008 for ceramic.

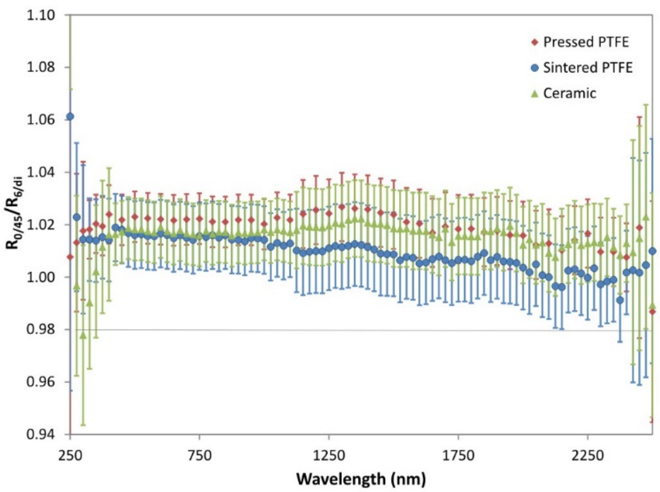

Fig. 5. The ratio $R_{0/45}/R_{6/\mathrm{di}}$ of spectral reflectance factor obtained using the 0/45 geometry to that obtained using the 6/di geometry as a function of wavelength λ of sintered PTFE, pressed PTFE, and ceramic samples. (The scale for this figure was chosen to depict the overall trend of the ratios across the spectral region; consequently, the ratio for the ceramic sample at 250 nm is beyond the scale of this figure.)

Table 3. Coefficients for the linear least-squares fits of the ratio $R_{0/45}/R_{6/\mathrm{di}}$ for the wavelength range 400 nm to 2500 nm of sintered PTFE, pressed PTFE, and ceramic samples.

Diffuser material	Slope	y-Intercept
Pressed PTFE	$-5.7\times10^{-6} \pm 3.0\times10^{-6}$	1.0273 ± 0.0042
Sintered PTFE	$-9.4\times10^{-6} \pm 2.7\times10^{-6}$	1.0222 ± 0.0039
Ceramic	$-2.5\times10^{-6} \pm 2.5\times10^{-6}$	1.0200 ± 0.0036

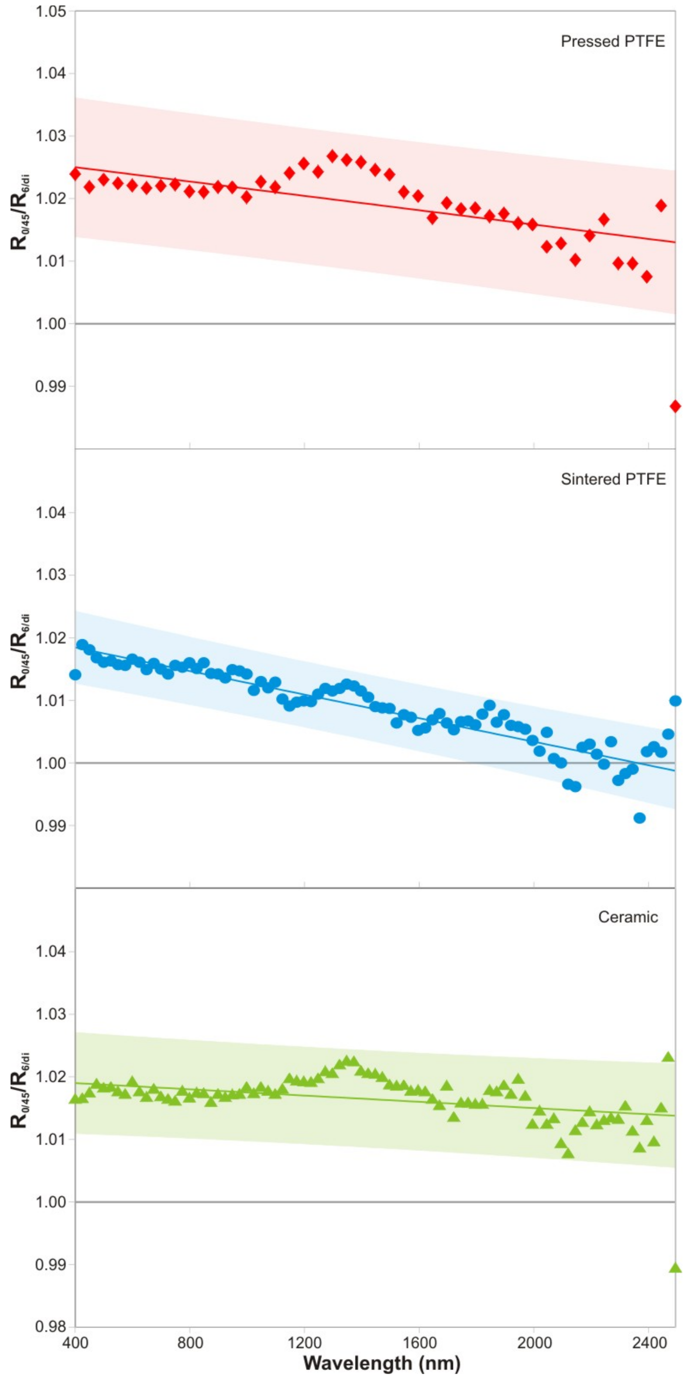

Fig. 6. The linear least-squares fits of the ratio $R_{0/45}/R_{6/di}$ of spectral reflectance factor obtained using the 0/45 geometry to that obtained using the 6/di geometry as a function of wavelength λ of sintered PTFE, pressed PTFE, and ceramic samples and their respective prediction bands (shaded areas).

5. Conclusion

NIST has disseminated the reflectance scale for many years through the calibration of reflectance standards. Until recently, the capability of measuring bidirectional reflectance was limited to wavelengths less than 1100 nm. However, the development of low noise, high-shunt resistance ex-InGaAs based radiometers has enabled the expansion of NIST's bidirectional reflectance capability to include wavelengths from 1100 nm to 2500 nm.

Using this new capability, the 0/45 reflectance factors of three materials commonly used for reflectance standards were determined from 250 nm to 2500 nm. All three materials exhibited reflectance properties considered desirable for reflectance standards, namely that the material is spectrally flat with high reflectance values. Choice of material for a reflectance standard then depends on factors such as cost, application, and environmental conditions.

Pressed PTFE is a low-cost option, accessible to any laboratory. A simple press can be used to create a sample from powdered PTFE, and reference values for the 45/0 reflectance factors of pressed PTFE from 380 nm to 770 nm are available [15]. Using the ex-InGaAs radiometer, NIST will be expanding this reference set beyond the visible region in a future publication.

Sintered PTFE is produced by a process of pressing and heating that transforms powdered PTFE into a solid, machinable, thermoplastic resin. The surface is durable and cleanable, unlike pressed PTFE. Its thermal and chemical stability have made it a popular choice for remote sensing applications, such as an in-flight calibration diffuser on satellite sensors. The ceramic sample used in this study was designed to be high-performing in terms of its durability and thermal stability. The ceramic sample is available in two forms, glazed and unglazed. While the glaze may provide protection from contaminants, this study only examined the unglazed ceramic due to its improved diffuse reflectance properties. Nevertheless, the ceramic sample may be a suitable alternative for in-flight diffusers due to its more spectrally flat features in the SWIR. Future work involves the characterization of its aging properties of ceramic due to UV exposure as compared to sintered PTFE.

Now that we have successfully demonstrated the capability to measure 0/45 reflectance factors beyond 1100 nm, NIST is developing the next-generation reflectometer, which will allow reflectance calibrations to be made at nearly any combination of incident and scattering angles over the full solar reflective region [17].

The authors gratefully acknowledge C. Cameron Miller of NIST and Jack Root of Mt. Baker Research L.L.C. for their helpful insights.

*Note: References are made to certain commercially available products in this paper to adequately specify the experimental procedures involved. Such identification does not imply recommendation or endorsement by the National Institute of Standards and Technology, nor does it imply that these products are the best for the purpose specified.

References

1. F. E. Nicodemus, J. C. Richmond, J. J. Hsia, I. W. Ginsberg, and T. Limperis, "Geometrical considerations and nomenclature for reflectance," NBS Monograph 160 (1977).
2. H. W. Yoon, D. W. Allen, G. P. Eppeldauer, and B. K. Tsai, "The Extension of the NIST BRDF Scale from 1100 nm to 2500 nm," Earth Observing Systems XIV, Proc. of SPIE, 7452, 745204 (2009).
3. P. Y. Barnes, E. A. Early, and A. C. Parr, "Spectral Reflectance," NIST Special Publication 250-48, U.S. Dept. of Commerce, March 1998.
4. H. W. Yoon, M. C. Dopkiss, and G. P. Eppeldauer, "Performance Comparisons of InGaAs, extended InGaAs, and Short-wave HgCdTe Detectors between 1 μm and 2.5 μm," Infrared Spaceborne Remote Sensing XIV, Proc. of SPIE, 6297, 629703 (2006).
5. J. H. Walker, R. D. Saunders, and A. T. Hattenburg, "Spectral Radiance Calibrations," NIST Special Publication 250-1, U.S. Dept. of Commerce, January 1987.
6. H. W. Yoon and C. E. Gibson, "Spectral Irradiance Calibrations," NIST Special Publication 250-89, U.S. Dept. of Commerce, July 2011.
7. ISO/IEC Guide 98-3:2008: Uncertainty of measurement – Part 3: Guide to the expression of uncertainty in measurement
8. B. N. Taylor and C. E. Kuyatt, "Guidelines for Evaluating and Expressing the Uncertainty of NIST Measurement Results," NIST Technical Note 1297 (1994).
9. K. D. Mielenz and K. L. Eckerle, "Spectrophotometer Linearity Testing Using the Double-Aperture Method," Applied Optics, 11, 2294 (1972).
10. J. Root, Mt. Baker Research L.L.C, 2921 Sylvan Street, Bellingham, Washington 98228-0370 (personal communication, 2014).
11. D. Hünerhoff, U. Grusemann, and A. Höpe, "New Robot-Based Gonioreflectometer for Measuring Spectral Diffuse Reflection," Metrologia, 43, S11-S16 (2006).
12. G. T. Georgiev, J. J. Butler, C. C. Cooksey, L. Ding, and K. J. Thome, "SWIR Calibration of Spectralon Reflectance Factor," Sensors, Systems, and Next-Generation Satellites XV, Proc. of SPIE, 8176, 81760W (2011).
13. W. H. Venable, J. J. Hsia, and V. R. Weidner, "Establishing a Scale of Directional-Hemispherical Reflectance Factor I: The Van den Akker Method," J. Research NBS, 82, 29 (1977).
14. V. R. Weidner and J. J. Hsia, "Reflection Properties of Pressed Polytetrafluoroethylene Powder," J. Optical Soc. of Am., 71, 856 (1981).
15. P. Y. Barnes, and J. J. Hsia, "45°/0° Reflectance Factors of Pressed Polytetrafluoroethylene (PTFE) Powder," NIST Technical Note 1413, U. S. Dept. of Commerce, July 1995.

16. "NIST/SEMATECH e-Handbook of Statistical Methods," http://www.itl.nist.gov/div898/handbook/pmd/section1/pmd132.htm, accessed 2/6/2015.
17. H. J. Patrick, C. J. Zarobila, and T. A. Germer, "The NIST Robotic Optical Scatter Instrument (ROSI) and its Application to BRDF Measurements of Diffuse Reflectance Standards for Remote Sensing," Proc. SPIE, 8866, 886615 (2013).